RSC Advances

ROYAL SOCIETY OF CHEMISTRY

www.rsc.org/advances

Solution Chemistry based Nano-structuring of Copper Dendrites for Efficient use in Catalysis and Superhydrophobic Surfaces

Rangarajan Bakthavatsalam[†], Subrata Ghosh[†], Ratul Kumar Biswas[†], Aayushi Saxena[†], Alagar Raja[‡], Musthafa Ottakam Thotiyl[‡], Sandip Wadhai[§], Arun G. Banpurkar[§], Janardan Kundu[†*]

[†] Physical and Materials Chemistry Division, CSIR-National Chemical Laboratory, Dr. Homi Bhabha Road, Pashan, Pune, Maharashtra, India, 411008.

[‡] Department of Chemistry, Indian Institute of Science Education and Research, Dr. Homi Bhabha Road, Pashan, Pune, Maharashtra, India, 411008.

[§] Department of Physics, Savitribai Phule Pune University, Ganeshkhind, Pune, Maharashtra, India, 411007

Abstract:

Despite its performance and economic advantages over Ag and Au, focused research efforts on nano-structuring of the Cu dendrites to fine tune their structure/morphology tailored towards efficiency enhancement of suitable applications has not been demonstrated. Reported here is a simple, versatile, environment-friendly, and galvanic replacement reaction based solution chemistry methodology to synthesize highly nano-structured copper dendrites targeted towards efficiency enhancement for desired applications. Here, copper is deposited galvanically on Al foil in the presence of NaCl/HCl wherein the chloride anions augment an uninterrupted replacement reaction. The growth process of Cu dendrites has been probed in detail. Presence of the acid, type of the Cu^{2+} precursor salt, Cu^{2+} ion concentration, surfactant concentration, and reaction temperature are all demonstrated to provide useful means of modulating surface structure/morphology of the dendrites. Notably, the dendrites formed in the presence of acid are found to be highly nano-structured. Moreover, it is also found that the morphology/structure of the obtained Cu deposit dramatically depends upon the choice of the Cu^{2+} precursor salt, a parameter that has been completely overlooked in the past. The acid induced nano-structuring of the dendrites is exploited for enhancing their efficiency in applications for catalytic reduction of para-nitrophenol and fabricating self-cleaning superhydrophobic surfaces. These nano-structured dendrites are demonstrated to

have highest ever normalized rate constant for the catalytic reduction reaction. Superhydrophobic surfaces fabricated using these dendrites demonstrate excellent self-cleaning abilities that show high contact angle (159^0) with low contact angle hysteresis (2^0). This facile synthetic strategy for fabrication of highly nano-structured Cu dendrites is expected to open up avenues for production of Cu based low cost functional nano/micro-materials.

Key words:
Copper dendrites, Galvanic replacement reaction, nano-structuring, catalysis, para-nitrophenol reduction, static contact angle, superhydrophobic surfaces, self-cleaning surfaces.

Author Information:

Corresponding Author
*E-mail: j.kundu@ncl.res.in

Notes: The authors declare no competing financial interest.

Introduction:

Metallic nanostructures of Group 11 elements (namely Cu, Ag, Au) have been extensively exploited for their unique optical, electronic, magnetic, and catalytic properties. [1-7] Tailoring their intrinsic and unique properties is achievable by tuning the size, shape, morphology, crystal phase composition of the metallic nanostructures.[6, 8, 9] These nanostructures, in comparison to their bulk counterparts, find interesting applications in catalysis, microdevices, electrical and thermal conduction, lubrication, fabrication of superhydrophobic surfaces, and plasmonic sensing.[6, 7, 10-13] With the advancement of wet-chemical synthetic techniques, it is now possible to controllably fabricate a variety of metallic nanostructures in solution. An important class of nanostructure that has recently been the focus of interest are the so called dendritic structures. In simple words, dendritic nanostructures are self-assembled, hierarchical, repetitive structures with main stem and many side branches resembling fern or bracken like structures. Consequently, these networked structures have high surface area, high conductivity, and can act as model system in the field of mathematics for understanding pattern formation. Dendritic nanostructures are believed to be formed under kinetic control, far from thermodynamic equilibrium growth conditions.[14, 15] Several growth mechanisms, such as diffusion-limited-aggregation (DLA) model,[16, 17] oriented attachment,[18, 19] nanoparticle aggregated self-assembly crystallization,[20-22] and anisotropic crystal growth[15, 23] have been proposed to explain the formation process. However, DLA and nanoparticle aggregated self-assembly crystallization mechanisms have been widely utilized to explain the growth process of these dendritic structures.

Amongst the group 11 metals, Copper dendrites are receiving the current attention due to low price/ earth abundance and unique enabling properties of metallic copper.[15, 24-34] Copper offers several economic and performance advantages over precious metals. The conductivity of copper is comparable to that of silver and 40% better than that of gold.[35] The stability of copper at high frequencies is better than gold or silver and it is compatible with most solder materials.[35] Although the inherent susceptibility of metallic copper to undergo oxidation has been cited as a difficulty in synthesizing copper nanostructures, many successful efforts have been reported on mitigating this issue of oxidation by utilizing protective coating/ligands/surfactants during synthesis of copper nanostructures.[36-39] Hence, high-purity, uniformly shaped, nano-structured Cu is highly desirable for use in the electronic industry. Research efforts are now being devoted for controllable fabrication of Cu based dendritic nanostructures for the development of functional materials that finds practical applications in cheap and effective catalysis, microdevices as nano-joints, electrical and thermal conduction, superhydrophobicity for self-cleaning surfaces, and SERS (surface-enhanced

Raman scattering) based biochemical sensing.

Copper dendrites have been fabricated by various routes: traditional electrochemical deposition,[24, 25] hydrothermal synthesis,[28, 40] electroless deposition method (Galvanic replacement reaction/GRR)[26, 27, 29, 30]. Of these synthetic routes, GRR based strategy (redox displacement reaction) is the preferred choice for the fabrication of dendritic nanostructures primarily due to the simplicity and versatility of the GRR process. Although GRR strategy has been extensively implemented for the synthesis of dendrites of Ag and Au but not much for Cu dendrites have been reported. In many of the existing reports on GRR based fabrication of dendrites, Cu dendrites were fabricated to showcase the generality of the synthetic strategy.[26, 30] Reports that specifically focus on the GRR based fabrication of Cu dendrites targeted towards particular applications are scarce.[26, 27] Most of the reports on fabrication of Cu dendrites, however, do not implement the various reaction parameters as effective handle to fine tune the structure/morphology of the dendrites. Interestingly, there exist no report on utilizing different Cu^{2+} precursor salts during the GRR fabrication of Cu dendrites. The effect of surfactant during the GRR deposition of Cu dendrites has also not been probed extensively. These reaction parameters (alone or in combination) are expected to have drastic influence on the shape/structure/morphology of the Cu dendrites that can immensely impact the efficiency of their applications. Hence, the primary objective of this work is to focus comprehensive research efforts on nano-structuring of Cu dendrites targeted towards efficiency enhancement of desired applications.

In a typical GRR process, metal ions (in a bath solution) of higher reduction potential undergoes spontaneous reduction at the expense of oxidation of a metal under-layer substrate with lower reduction potential, without the application of external current or reducing agents. Generally utilized metal under-layer substrate with low reduction potential includes Mg foil/powder, Al foil, Zn foil. Al foil being economically viable and having lower reduction potential ($E_{0\ Al^{3+}/Al}$ = -1.67 V vs. S.H.E) than most metal ions are excellent choice as under-layer substrate. However, utilizing Al foil for deposition of metals of higher reduction potential inevitably fails due to the formation/presence of thin layer of Alumina (Al_2O_3) that acts as a insulating barrier to the GRR process. To overcome this difficulty, fluoride ions (F^-) were demonstrated as a reagent that dissolves the alumina layer thereby leading to the uninterrupted proceeding of the galvanic displacement reaction.[11, 30] In particular, Li *et al* demonstrated a facile and uninterrupted galvanic replacement route to produce metal dendrites on commercial

aluminum foil in the presence of NaF or NH_4F as the alumina etchant.[30]. Undoubtedly, such a strategy of using commonly available/ low cost reagents (NaF or NH_4F) help in large scale production of the nano-materials. Nonetheless, the process involves fluoride anions that can strongly bind to metal dendrites and affect their performance negatively. Fluoride ions are also considered to be highly toxic.[41] Moreover, this process[30] of fluoride-assisted galvanic replacement synthesis of dendrites on Al foil takes a long time (10 hrs.).[26, 41]

Here, we report a simple yet versatile, rapid, environment-friendly, and uninterrupted solution chemistry based methodology to synthesize nano-structured copper dendrites by the galvanic displacement route on Al foil with the use of NaCl/HCl as the etching reagent for alumina. The chloride anions can dissolve alumina by forming $[AlCl_4]^-$ anion that can be easily washed off rendering the process environment-friendly. Here, GRR proceeds along with the reaction of the Al substrate with the acid that produces hydrogen gas. The produced hydrogen gas maintains a local oxygen free environment thereby suppressing oxide formation. This chloride assisted methodology is easily scalable with high yield obtained in less than 2 hours of total reaction time. Notably, the presence of the acid in the system is found to be an effective handle that can highly nano-structure the morphology of the fabricated dendrites. We also explore the effect of choice of Cu^{2+} precursor salts such as $CuSO_4$ and $Cu(NO_3)_2$, (a parameter that has largely been ignored/overlooked in the past reports of Copper dendrites)[15, 24-30], surfactants, and reaction temperature on the yield and morphology of the copper dendrites obtained. Surprisingly, we find that the choice of precursor Cu^{2+} salt has profound effects on the yield/morphology of the copper deposits thus obtained. These acid induced nano-structured dendrites are demonstrated to be highly useful for applications in: 1) catalytic reduction of 4-Nitrophenol, and 2) fabricating superhydrophobic surfaces. These dendrites act as efficient catalysts with highest ever reported rate constant for the catalytic reduction reaction. These dendrites also exhibit superhydrophobicity with excellent self-cleaning abilities. The material properties of these dendrites are largely shaped by the solution chemistry based nano-structuring which enhances their efficiency in various applications.

Experimental:

Al foil (99.5%, thickness: 0.14 mm), $CuSO_4$ (>99.5%), $Cu(NO_3)_2$ (>99.5%), $CuCl_2$ (>99.5%), Na_2SO_4(>99.5%), NaCl (>99.5%), HCl (AR) were all purchased from Loba Chemie. Sodium borohydride (>98%), Polyvinylpyrrolidone (PVP 55 K), PDDA (Poly (diallyldimethylammonium chloride)) (20 wt. % in H_2O), Poly (4-Styrenesulfonic acid)(M_w ~ 75,000) and n-dodecanethiol (≥98%) were purchased from Sigma Aldrich and $NaNO_3$

(>99.5%) was purchased from Merck. Commercial Cu powder (99.5 %, spherical, mesh size: -100) was bought from Alfa Aesar. Milli-Q water (resistivity > 18 MΩ· cm) has been used throughout for carrying out the reactions while Ethanol (99%) has been used for washing samples.

Aluminium foils were cut into 1x1 cm^2 and cleaned by sonicating in ethanol and water sequentially for two minutes each. The copper dendrites were synthesized by immersing the cleaned Al foil in 2 ml solution mixture of desired concentration of $CuSO_4$/$Cu(NO_3)_2$ and NaCl/HCl in a polypropylene reaction vial of 5 ml volume. The reaction proceeds with bubbling and deposition of metallic copper on the Al foil. The reaction is stopped after 2 hours by removing the Al foil from the reaction solution mixture. After the completion of the reaction, the copper deposits are separated from the foil and cleaned with deionised water and ethanol thoroughly. For XRD, XPS, and catalytic activity studies, the cleaned copper deposits were dried in a vacuum oven at 60 °C for 4-6 hours. For SEM analysis, the deposits on the Al foil were cleaned by successive washing in water and ethanol before they were directly imaged on the Al foil. For TEM and HRTEM measurements, the foil containing the deposits were sonicated to disperse the copper structures in ethanol before drop casting on TEM grids (carbon coated copper grids, 200 mesh size).

Catalytic Activity:

To test the catalytic activity of the prepared Cu dendrites and commercial Cu powder, the reduction of 4-nitrophenol in excess $NaBH_4$ was studied spectrophotometrically. The as prepared Cu dendrites were washed successively with water, ethanol, dilute NaOH, and water and ethanol to remove any remaining salt/acid. To 20ml of 1 mM 4-nitrophenol, 10 ml of 0.4 M $NaBH_4$ was added and specified amount of Cu dendrite catalyst was added at the start the reaction. Once the catalyst was added the reaction was monitored by spectrophotometer. 4-nitrophenol (4-NP) on addition of $NaBH_4$ shows a strong absorption at 400 nm. The color of the solution turns from pale to bright yellow due to formation of 4-nitrophenolate ion. In the presence of the catalyst (Cu dendrites), the solution color slowly changes from yellow to colorless. This is monitored (as a function of time) by observing the intensity of the 400 nm peak in UV-Vis spectra and the concomitant increase of the 300 nm peak corresponding to the formation of 4-aminophenol as the product. The catalytic assay of the commercial Cu powder was run as described above except

for using 3ml of 1mM 4-NP, 10ml of 0.4 M $NaBH_4$ and 10 mg of the Cu powder. These catalytic reactions were repeated at least 5 times to ensure reproducibility.

Cyclic Voltammetry:

CV experiments were performed in a BASI Epsilon cyclic voltammeter with N_2 purging. The experiment was performed in a typical three electrode system with Glassy carbon as working electrode, Ag/AgCl (E_o = 0.197 Vs SHE) as reference and Platinum as counter electrode. For copper electrodeposition, a solution of 50 mM $CuSO_4$, and 100 mM Na_2SO_4 was used as a background electrolyte to mitigate issues of uncompensated resistance. The Scan rate was fixed at 20 mV/sec. CV scan was done at various switching potentials ranging from -500 to -750 mV vs Ag/AgCl electrode. For comparison purposes, similar experiments were done with same parameters but using copper nitrate instead of copper sulphate as the Cu^{2+} precursor.

Superhydrophobic surface preparation:

Glass slides are cut into 1x1 cm^2 immersed in a 3:1 mixture of sulphuric acid and hydrogen peroxide for 4-5 hrs. It is then washed with copious amounts of DI water and dried in air. To deposit copper dendrites on glass substrate, a multi-layer of charged polymer was initially coated on the cleaned glass slides. This was achieved through layer by layer deposition process. The cleaned glass substrate was immersed in a 5% PDDA solution for 10 mins followed by rinsing with water and drying under nitrogen stream. To coat a layer of PSS onto this substrate, it is immersed in a solution of 5% PSS for 10 mins and washed with DI water and dried. Then another set of layer of PDDA-PSS was obtained in the same way. This process was repeated 2-3 times to obtain desired number of layers. The copper dendrites were then drop casted on these slides and dried in air. The Cu Coated glass slides were then immersed into a 100 mM ethanolic solution of n-dodecanethiol for 24 Hrs. It is then washed with ethanol and dried in air.

Static water contact angle (SCA) and contact angle Hysteresis (CAH) measurements:

The equilibrium contact angle for water droplet on several hydrophobic surfaces was determined using Optical contact angle goniometer (OCA). A CCD camera was attached with the variable magnification microscope (1-5X). A sessile droplet was gently casted on surface using precision needle attached to water delivery for precise control of drop volume. A micro-syringe pump (pico-plus Harvard) is employed for precisely controlling the water drop volume The sessile drop was back illuminated using diffused LED lights. The CCD camera, water drop and backlight were kept co-axially and fixed on the rigid stand. Using syringe pump, a water drop of nearly 8 μL was

deposited on superhydrophobic surface. This was "sessile drop needle in" arrangement and the drop image was constantly monitored and analyzed using software SCA 20 (dataphysics, Germany). Contact angle was measured using elliptical fitting to the droplet boundary. The experiment was repeated many times on same sample at different places.

Advancing receding contact angle (ARCA) goniometry was utilized for the real time measurement of the contact angles of water drop characterizing the hysteresis. The water drop volume was controllably increased from 10 µL to 20 µL at the rate of 3 µL /min. and then brought to its initial volume (10 µL). During this process, the contact angle of water drop was measured and analyzed using SCA 20 software (dataphysics, Germany). The difference between the advancing and the receding contact angle is the measured contact angle hysteresis.

Characterization:

The as-prepared products are characterized by X-ray diffraction (XRD) using a PAN analytical X'Pert Pro equipped with Cu Kα radiation (λ = 1.5406 Å), field emission scanning electron microscope (FE-SEM) images were taken using a ZEISS, Ultra Plus instrument. XPS surface analysis was performed using Multi-Lab, ESCA-3000 (VG Microtech, England). Transmission electron microscope images were obtained from Tecnai T20 TEM operating at an accelerating voltage of 200 kV. HRTEM images were obtained using FEI Tecnai G2 30 S-Twin instrument operating at 300 kV. UV-Vis spectroscopy was done using a Shimadzu UV-3600 plus UV-Vis-NIR spectrophotometer. Real time video of water droplet rolling off of the superhydrophobic surface was captured using Sony HDR CX 160 Handycam.

Results & Discussion:

Deposition process: We have performed environment-friendly, rapid, very simple electroless deposition, utilizing uninterrupted galvanic replacement reaction (GRR) strategy, for fabricating Cu dendritic micro/nano-structures on Al foil without using fluoride anions. Dendrites are formed during the galvanic deposition of $CuSO_4$ on Al foil in the presence of NaCl/HCl. This GRR deposition of Cu on Al foil does not proceed at all in the absence of chloride anions (See Figure S1, Electronic Supporting Information). Driven by the differences in the redox potentials, Cu^{2+} ions are spontaneously reduced to metallic copper at the expense of oxidation of Al to Al^{3+} ions in the presence of the chloride anions. The dissolved dioxygen in the aqueous solution can undergo reduction to form hydroxyl anions

(E_0 O_2/OH^- = 0.4 V) that can lead to the formation of $Al(OH)_3$ acting as a barrier to the GRR process. However, the presence of the Cl^- anions help complex the released Al^{3+} ions in the form of soluble $[AlCl_4]^-$ anion, thereby preventing formation of undesired alumina barrier layer. Considering the harmful/undesired effects of flouride anions, as mentioned earlier, we utilize chloride anions for performing uninterrupted GRR. The presence of acid during the GRR stops the production of hydroxyl ions and produces H_2 gas that maintains a local oxygen free environment which prevents oxide formation and hence augments the uninterrupted GRR process. A schematic of such processes is shown in Figure 1a. The simplicity, easiness, eco-friendliness, and versatility (high yield > 94 %, short reaction time < 2 hours) are the major attractions of the utilized solution chemistry based facile methodology for controllable fabrication of Cu dendrites on Al foil.

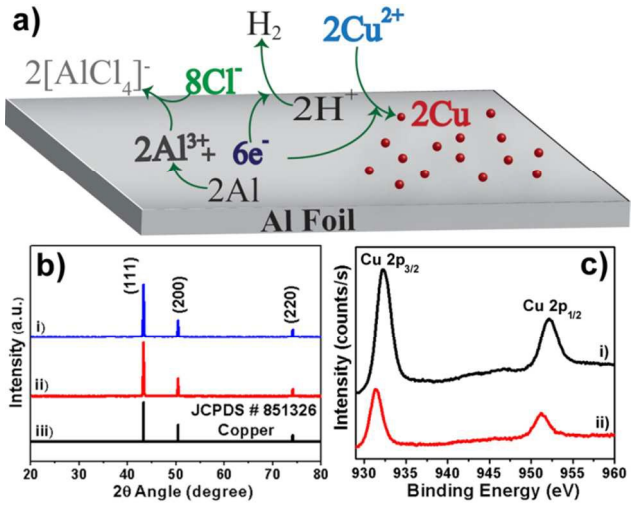

Figure1: a) Schematic illustration (not to scale) of the various reactions occurring during the GRR deposition of metallic Cu on Al foil in presence of Cl^- anion; b) XRD pattern (stacked) of Cu dendritic structures prepared from i) $CuSO_4$ (50 mM) + NaCl (100 mM). ii) $CuSO_4$ (50 mM) + HCl (100 mM). iii) Standard JCPDS pattern of Cu; c) XPS spectra (stacked) of Cu dendrites prepared from i) $CuSO_4$ (50 mM) + HCl (100 mM), and ii) $CuSO_4$ (50 mM) + NaCl (100 mM).

Elemental and Phase composition:

XRD: The elemental composition, purity and phase structure of the as prepared products were analyzed by X-ray diffraction (XRD). Figure 1b shows the XRD of the Cu dendrites prepared using $CuSO_4$ (50 mM) + NaCl (100 mM); and $CuSO_4$ (50 mM) + HCl (100 mM). As shown in the Fig. 1b, XRD pattern for both the samples reveal sharp peaks which are indexed to the diffraction from the {111}, {200}, and {220} of face-centered cubic (fcc) copper (JCPDS file # 851326). The sharp peaks indicates high crystallinity of the prepared Cu dendrites. No other peaks of copper oxides were discernible suggesting the high purity of the material. It is also observed that the intensity of (111) is much stronger as compared with the standard intensity of (200), indicating that most of the branches of the dendrites are parallel to the (111) habit plane, and thus their (111) facets tend to be preferentially oriented parallel to the surface of the supporting substrate.

XPS: XPS is a well-known technique for determining the surface elemental composition of a solid, i.e., its oxidation state and/or surface chemistry. Figure 1c depicts the XPS spectra of the Cu dendrites prepared from i) $CuSO_4$ (50mM) + HCl (100mM), and ii) $CuSO_4$ (50mM) + NaCl (100mM). For the Cu dendrites prepared in presence of HCl, XPS spectra present peaks at binding energies of 932.3 eV and 952.2 eV for Cu $2p_{3/2}$, and Cu $2p_{1/2}$ respectively. For the Cu dendrites prepared in presence of NaCl, these peaks appear at 931.3 eV and 951.2 eV respectively. The presence of these peaks clearly indicates that the surface of these dendrites are of elemental copper. For both these spectra, we do not see any features in the 940 - 950 eV range where satellite peaks of Cu oxides (cuprous/cupric) are known to appear. This clearly demonstrates the phase purity of the prepared metallic Cu dendrites with no detectable signs of oxides on the surface. Noteworthy here is the fact that Cu nanostructures are notorious to undergo oxidation that compromises it's properties and efficiency in its applications. Hence, it is imperative to establish that the as prepared Cu dendrites do not undergo oxidation. XRD and XPS together confirms no detectable oxidation of the fabricated Cu dendrites.

Structure and Morphology:

Structure and morphology of the prepared products were characterized using SEM, TEM/SAED analysis. Figure 2 shows the SEM images of Cu dendrites fabricated at room temperature using $CuSO_4$ (50mM) and NaCl/HCl (100 mM) exhibiting typical dendritic structure. The low-magnification SEM image (Fig. 2a,d) reveals that a large quantity and good uniformity of Cu dendrites can be exclusively obtained using this approach. The micro/nano-structured dendrites consist of a pronounced central backbone with many symmetrical primary and secondary

branches. (Fig. 2b,e). It is also seen that not all the primary branches are fully developed. The coexistence of the big and small primary branch is observed because the branch alignment experiences a space-limited growth. SEM images (Fig. 2c,f) and TEM images of single dendrites (Fig. S2 a,b: Electronic Supporting Information) clearly show that the primary branches are parallel to each other emerging at 55° - 60° angle with respect to the central backbone and the primary branches preferentially grow along two definite directions rather than randomly ramified growth. A closer view of the SEM images clearly reveal that the central backbone, and the various branches are composed of aggregate of small nanoparticles. Moreover, the discontinuous concentric ring-like pattern of the selected area electron diffraction pattern (SAED), as shown in insets to Figure S2 a,b (Electronic Supporting Information), indicates the characteristic of single crystal structure of cubic Cu.

It is interesting to compare and contrast the structure/morphology of the dendrites prepared using NaCl and HCl as prepared with 50 mM $CuSO_4$ and 100 mM NaCl/HCl. The dendrites prepared using NaCl (CuS_Na) are observed to be dense and much longer in dimensions while the dendrites prepared using HCl (CuS_H) are observed to be slender and shorter. The average lengths of the dendrites for CuS_Na are ~ 20 μm as compared to ~10 μm for CuS-H. The secondary branches in case of Cus_Na are seen to be fused and not crisply divided into individual leaves. However, for the Cu_H, the secondary branches are clearly seen with no fusion and appear crisply demarcated. Experimentally, the utilization of HCl leads to the observed differences in the extent of fusion and surface nano-texturing (surface area) as compared to the use of NaCl. Hence, we believe that the presence of the acid during the GRR process is an effective handle that can tailor the surface area and morphology of the fabricated dendrites. The acid present in the reaction system not only helps mitigate oxidation issues, but it also acts as a competitive channel working against GRR deposition of Cu due to the reduction of H^+ to H_2 gas by the Al foil. This acid based competition, however, is a relatively weaker channel than the GRR based Cu^{2+} reduction ($E^0_{H+/H2} = 0.0$ V; $E^0_{Cu2+/Cu} = 0.33$ V). Due to this weaker competition , the GRR deposition rate is expected to slightly decrease for HCl system when compared to the scenario for NaCl. The relatively higher nucleation rate while using NaCl might lead to higher growth rate that can result in fusion of the nanoparticles. However, for the HCl system, the lower nucleation and growth rates would provide sufficient time necessary for reorientation and preferred attachment of the nano-particles amongst each other, as dictated by minimization of surface energy, that might mitigate random fusion of

nanoparticles while the growth of branches in the dendritic structures. This observed increased surface area for the dendrites prepared with HCl as compared to NaCl is an excellent feature of this approach as many of the applications of dendrites (such as catalysis, wettability) crucially depends on the available surface area, and trapped air fraction in these micro/nano structures. This difference in the morphology is heavily exploited for demonstrating markedly different efficiencies in applications of these dendrites in catalysis and superhydrophobic surfaces as presented in the later section of this report.

Notable here is that the Cu dendrites fabricated here have $[Cu^{2+}] : [Cl^-] = 1: 2$. We have also tried the 1: 3, 1:5, and 1:10 ratio to obtain Cu deposits on the Al foil. The reaction system is found to be highly robust and tolerant towards small variation of the chloride concentration. Dendritic structures are still the major product at 1:5 ratio. Only at a much higher $[Cu^{2+}] : [Cl^-]$ ratio of 1:10, we observe changes in the morphology of the Cu deposits. SEM analysis of the Cu deposits, as shown in Figure S3 (Electronic Supporting Information), shows that along with Cu 'dendritic like' structures, we evidence the formation of 'micro rod' like structures in modest relative amount. These faceted rod like structures are smooth and long (~ 20 microns) with progressive tapering at the tips (~ 1 micron 'diameter'). These smooth rod facets are found to be decorated with tiny Cu nanoparticles that acts as sites for further growth resembling much like "cactus" structures. The seemingly 'dendritic like' structures are found to have different structure/morphology when compared to structures shown in Figure 2. Here in the case of increased $[Cu^{2+}] : [Cl^-]$, the dendritic like structures have less dense primary branching with no signs of secondary branching. Moreover, there is three dimensional growth of the primary branches from the central trunk. Also, these primary branches look more like smooth micro rods with clearly observable faceting. The observed differences in the structure/morphology of the Cu deposit obtained by varying the Cu^{2+}/Cl^- ratio can be attributed to the increased $[Cl^-]$. Shao *et* al,[25] Wu et al,[42] have previously demonstrated this increased faceting of Cu nanostructures with increased $[Cl^-]$. This chloride assisted growth with increased faceting has been attributed to preferential binding and stabilization of the chloride anion on to (100) planes of the developing Cu nanostructure.[25] We believe that similar chloride assisted growth might be operative in our case at increased $[Cu^{2+}] : [Cl^-]$ ratio.

In order to test this, we have attempted the GRR based deposition of Cu on Al foil utilizing $CuCl_2$ as the precursor. The obtained morphology of the Cu deposit, shown in Figure S4 (Electronic Supporting Information), is clearly composed of dendritic like structures with sparse primary branches and no secondary branches. The growth of the primary branches is three dimensional and these branches are smooth faceted rods. The obtained morphology

utilizing $CuCl_2$ is very similar to structures obtained using $CuSO_4$ with added excess chloride (sulphate: chloride = 1:10; Figure S3). We think that in case of $CuCl_2$ precursor, the chloride anions, adsorbing preferentially on 100 facet of the developing Cu nanostructures, dictates morphology of the dendrites with faceted micro rod like structures developing as the primary branches. Here, one might consider the $CuCl_2$ system and $CuSO_4$ with added chlorides (Cu^{2+}: Cl^- = 1:2) to be similar and to yield similar morphology. However, the obtained structures with these two systems are very different (Figure S4 vs. Figure 2 a-c respectively). The only difference in the chemical composition of the system lies in the presence of sulphate anions that are known to bind to developing metallic nuclei[43]. Hence we believe that, in the case of $CuSO_4$ and excess chloride (sulphate: chloride = 1:2), the sulphate anions can strongly bind to developing Cu nanostructures even in the presence of chloride anions and leads to the formation of dendritic structures shown in Figure 2 a-c. Only at a much higher chloride amounts (sulphate: chloride > 1:10), the binding ability of chloride anion surpasses that of the sulphate anion and the morphology is dictated by the adsorbed chloride anions leading to the formation of smooth faceted rod like structures as shown in Figure S3.

We have also varied the amount of HCl in the reaction system by altering the [Cu^{2+}] : [HCl] ratio as 1:2, 1:5, 1:10, and 1:20. Again, the reaction system is surprisingly found to be highly robust and tolerant towards small variation of the HCl concentration. Dendritic structures are still the major product at 1:5 ratio. Only at a much higher [Cu^{2+}] : [HCl] ratio of 1:10 and above, we observe changes in the morphology of the Cu deposits. SEM analysis of the Cu deposits, as shown in Figure S5 (Electronic Supporting Information), shows that along with Cu dendritic structures we also observe a modest (~25 %) yield of wire like structures. The dendritic structures obtained here are smaller in sizes measuring ~ 5-7 microns with less developed secondary side branches. This subtle morphology change in the dendritic structure along with the formation of wire like structures constituted of small aggregated particles indicates the "slowness" of the GRR reaction when carried out in presence of higher amount of acid. The restrained nucleation and growth leads to the formation of incomplete dendrites with central trunk being composed of aggregated Cu nanoparticles. Cu nanoparticles are formed on the Al foil along with evolution of hydrogen gas as observed during the experiments. However, the presence of relatively higher amount of acid (Cu^{2+}: H^+ = 1:10), opens up the weaker H^+/H_2 competitive channel, that leads to decreased nucleation and growth and affects the morphology/structure thereby forming the rough wire like Cu deposits. It is worth pointing out here that at this increased amount of acid (Cu^{2+}: HCl = 1:10), there is a concomitant increase of the chloride amount. This increased chloride amount manifests increased faceting only weakly as observed by the SEM analysis. Although we do not understand why the

increased chloride amount would not show increased faceting, but we think that the copious evolution of H_2 gas might play a role in this.

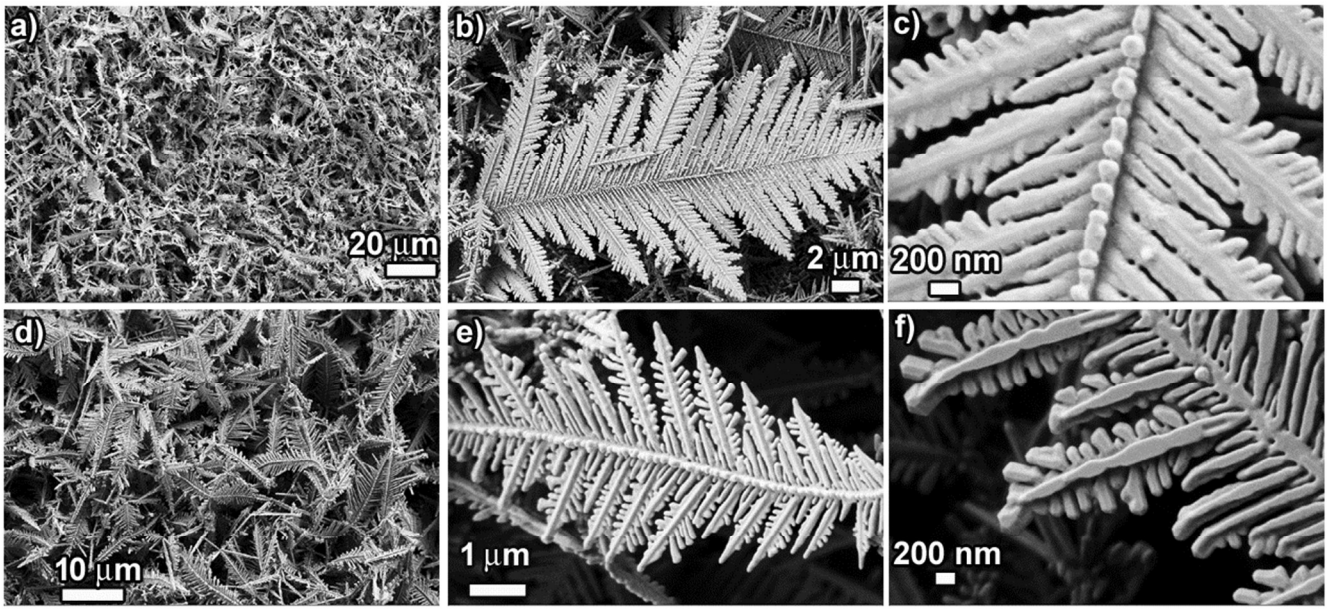

Figure 2. a), b) & c) FESEM image of Cu dendritic structures prepared at room temperature from $CuSO_4$ (50 mM), NaCl (100 mM) at different magnifications (**CuS_Na**); d), e) & f) FESEM image of Cu dendritic structures prepared room temperature from $CuSO_4$ (50 mM), HCl (100 mM) at different magnifications (**CuS_H**).

Growth process of dendrites:

In order to gain insight into the growth process of the dendrites, we monitored the time dependent evolution of morphology of Cu structures/dendrites through SEM investigation. Figure 3 (a-j) shows the SEM images of the products obtained at various reaction times (5 s, 10 s, 25 s, 45 s, 60 s, 2 mins., 3 mins., 5 mins., 9 mins., 60 mins. respectively). It is clearly observed that the initial stage of the reaction (5 s) involves formation of Cu "microparticles" on the surface of the Al foil. It is expected that tiny Cu nanoparticles rapidly nucleate on the surface of Al foil followed by further nucleation of Cu on these existing nanoparticles. The Ostwald ripening and/or migration of the nanoparticles and their coalescence leads to the formation of the as observed "microparticles" on the Al foil surface. As the reaction time increases (5-25 s), these "microparticles" act as the center on which 3D growth along the vertical direction occurs selectively. Again here, homogenous nucleation is suppressed and successive nucleation events occur on the existing Cu structures. Interestingly, as depicted in the inset of Fig. 3 c,

these vertical rod like structures are seen to be composed of tiny Cu nanoparticles stacked one on top of another. This also indicates that nanoparticles self-assemble/aggregate amongst themselves after achieving preferred relative orientation. These clusters of rod-like structures, growing vertically outward from the surface, further turns into "flowery" structures as can be seen at the end of 45 s of reaction time. The first sign of dendritic like structure is clearly visible at 45 s of reaction time (Fig. 3 d inset).

At about 1 min of reaction time, these flower like structures have grown both in size and in number and resembles "bush" like structure. As can be seen from Figure 3 e, these "bushes" have branches all over the surface of the Al foil and are highly interconnected to the nearby bushes. The inset in Figure 3 e indicates that the central trunk and its primary branches are getting into shape that would lead to the formation of dendritic structures. It is important to note here that the structure shown as the inset of Fig 3 e is clearly composed of nanoparticle self-assembled/aggregated amongst each other. By the end of 2 minutes of reaction time, the whole surface of the Al foil is covered with a mat of structures that look like the basic framework of dendrites. For reaction time of 2 minutes and above, the "bush" like structures are completely invisible due to the heavy growth and huge number of interconnections of the branches. The Al surface is now dominated by structures that are composed of the central trunk with growing primary side branches. From here on, we essentially find the growth of these central trunk and branches as the reaction time increases due to further nucleation events. At the end of 3 minutes of reaction time we can clearly see the central trunk being completely formed and the primary branches starting to lengthen. Interestingly, the incoming copper nanoparticles from the fresh nucleation event attach themselves on the tip of these primary branches thereby leading to their growth as shown in Fig. 3 g. Furthering the reaction time shows the growth of the primary branches and at the end of 9 minutes smooth and long primary branches are already formed. With further reaction time, we see the evolution of the secondary branches from the primary branch. These secondary branches are observed to be highly separated from each other and the structures obtained at 60 minutes reaction time are fully grown dendrites that are smooth, highly symmetrical with striking self-similarity. One of the common event that occurs throughout the whole growth process of the dendrites is the nanoparticle aggregation with self-assembly/preferred orientation.

Typically, DLA mechanism is proposed as the growth mechanism of dendrite formation. However, oriented attachment (OA), and nanoparticle-aggregated self-assembly crystallization mechanism has also been frequently

used to rationalize the dendrite formation mechanism. It is understandable that structure formation during dendrite growth is a complex many-body problem where various factors contribute to crystal growth and any single mechanism can only explain a part of the dendrite formation process. In our scheme of reactions where we clearly, see evidences of nanoparticle-aggregated self-assembly crystallization, we believe that both DLA and nanoparticle-aggregated self-assembly crystallization mechanism are relevant. The DLA model includes a single cluster to which additional particles attach once they reach a site adjacent to the edge of the cluster.[44] Tiny Cu nanoparticles that are formed initially on the surface of Al foil undergo surface migration and reorientation to form larger clusters. Concurrently, the growing Cu nuclei tend to deplete precursor ions near the Al foil surface that sets up concentric diffusion fields around the growing Cu clusters.[45] With further reaction time, the amount of the reactants decline that greatly decreases supersaturation and restrains nucleation events. Driven by the need to minimize surface energy, these small Cu clusters undergo reorientation, aggregation, and self assembly into rod like structures that act as further nucleation sites. These rod like structures further grow during the course of the reaction whereby successive nucleation occurs heterogeneously and the added nuclei undergoes stacked aggregation with preferred orientation giving the impression of self assembled nanoparticle aggregates. Further nanoparticle deposition and oriented aggregation through self assembly leads to the development of directed dendritic structures with central trunk and branches (primary, secondary) as governed by the DLA model. The whole process of dendrite formation is an interplay of DLA mechanism as well as nanoparticle-aggregated self assembly crystallization mechanism. This proposed mechanism is consistent with the previous reported mechanism of nanoparticle-aggregated self-assembly crystallization.[18, 46, 47] In addition, Ostwald ripening also plays an important role in forming a smooth surface and regular shape of the final crystal.[48]

HRTEM analysis of the completely formed dendritic structure was performed to gain insight into the preferred orientation within the dendrites. Figure S6 (Electronic Supporting Information) shows the images from the highlighted regions of the central trunk, and the primary branch of the dendrites. The image (Figure S6 b) taken from the tip of the central trunk shows obvious fringes with a ~0.21 nm inter-planar separation corresponding to the {111} planes. This indicates that the growth direction of the central trunk is along ⟨111⟩. The Figure S6 c shows a typical image recorded from the tip of the primary branch of the dendrites. Interestingly, fringes with inter-planar spacing of ~ 0.21 nm is also found here indicating that the growth direction of the primary branch is also along

⟨111⟩. This implies that the Cu dendrites grow along a preferential direction with preferred orientation within the dendrites.

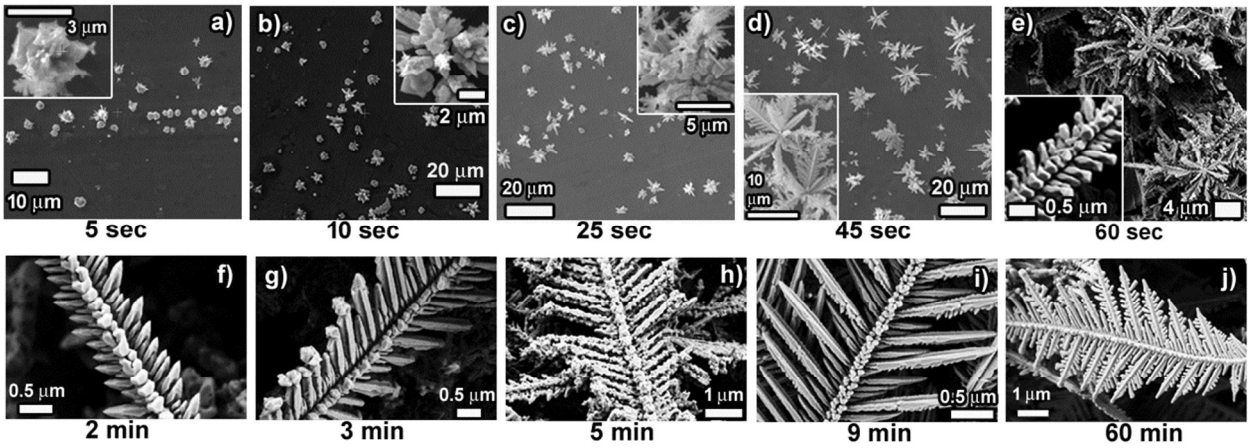

Figure 3. SEM investigation of the morphological evolution of Cu dendrites, as a function of Al foil immersion time, in a solution mixture of $CuSO_4$ (50 mM) and HCl (100 mM) for a) 5 seconds, b) 10 seconds, c) 25 seconds, d) 45 seconds, e) 60 seconds, f) 2 minutes, g) 3 minutes, h) 5 minutes, i) 9 minutes, and j) 60 minutes respectively. The insets in a)-e) show higher magnification images of the structures formed.

Effect of altering various reaction parameters on structure/morphology of Cu dendrites:

Various reaction parameters are expected to effect the structure and morphology of the Cu dendritic structures. Reaction temperature, reagent concentrations, presence of surface modifying agents (surfactants) would have a strong influence in shaping the morphology of the dendrites. We have systematically probed the effect of altering these reaction parameters on the structure/morphology of the Cu dendrites. It is important to note here that very few reports in the literature discuss the effects of these reaction parameters on the structure/morphology of the products thus obtained. Moreover, to the best of our knowledge, the effect of choice of Cu^{2+} precursor solution on the structure/morphology of the dendrites is reported here for the first time for Cu dendrites.

Amount of $CuSO_4$: We have probed the effect of amount of $CuSO_4$ on structure/morphology of the Cu dendrites obtained keeping the ratio of Cu^{2+} : Cl^- at 1:2. Figure 4 below shows the structure/morphology of the obtained Cu dendrites from $CuSO_4$ (25 mM) and NaCl/HCl (50 mM). A direct comparison of the SEM images as shown in Figure 2 and Figure 4 reveals the effect of amount of $CuSO_4$ on the structure and morphology of the obtained Cu dendrites. Clearly for the NaCl system, a decrease in the amount of $CuSO_4$ is accompanied by the formation of less

developed dendritic structures (Fig. 4 a,b) with lower overall yield. Unsurprisingly, the structures are shorter, less dense, and the growth of the primary and the secondary structure is incomplete as compared to the case with higher $CuSO_4$ concentration (Fig. 2 a, b, c) where the dendrites are longer, denser and fully formed. The reduced amount of $CuSO_4$ would lead to lowering of the nucleation and growth rate that might lead to the formation of less developed and shorter dendritic like structures as found in Figure 4 a, b. On the other hand, a comparison of structures obtained using HCl with different amount of $CuSO_4$ presents interesting findings. Even for the system with lower $CuSO_4$, the dendrites that are formed are very similar to the dendrites formed at higher $CuSO_4$ amount as revealed by analysis of the low magnification SEM images (Fig. 2 d, Fig. 4 c). However, a closer look at the high magnification SEM images (Fig. 2 e, Fig. 4 d) reveals the differences in the morphology of the Cu dendrites obtained with different $CuSO_4$ amounts. The secondary branches are not developed for the lower $CuSO_4$ amount case. The aggregation of smaller nanoparticles to form the primary branches are clearly observable demonstrating the effect of lowered $CuSO_4$ amount. The expected lowered nucleation and growth rate for this system is manifested in the form of "slowness" of the reaction where the primary branches are now barely formed with no signs of the evolution of the secondary branches. Hence, these structures appear more rough than the structures obtained at higher $CuSO_4$ amount. Consequently, these dendrites are anticipated to have higher surface area with increased nano-structuring. Such aspects make them very attractive towards variety of applications (catalysis, wettability, SERS sensors).

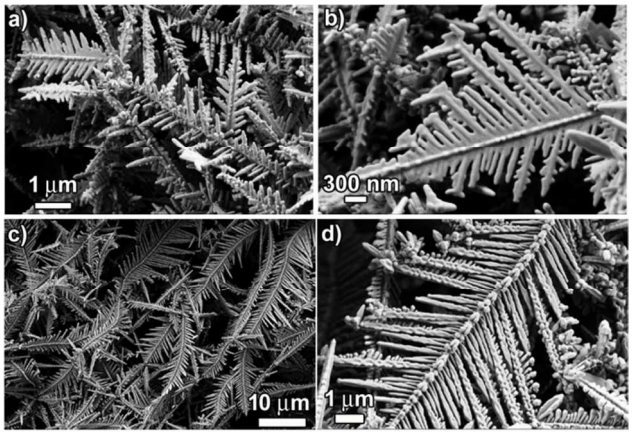

Figure 4. a), b) FESEM image of Cu dendritic structures prepared from $CuSO_4$ (25 mM), NaCl (50 mM) at different magnifications; c), d) FESEM image of Cu dendritic structures prepared from $CuSO_4$ (25 mM), HCl (50 mM) at different magnifications.

Presence of Surfactants: Presence of surfactants during the GRR deposition of Cu structures on Al foil can have significant influence on the shape, size, and morphology of the obtained products. Typically surfactants are utilized as a shape directing agent because of their affinity to preferentially bind and stabilize a specific facet of a developing nanoparticle. During the kinetically controlled fast growth of dendrites, processes such as nucleation, migration, and self assembly through preferred orientation dominates the growth mechanism. The rate at which these events occur relative to the rate at which the surfactant binds to the nucleating nanoparticle can have profound effect on the process of dendrite growth. Moreover, surfactant coating might diminish the drive for fusion based self assembly of nanoparticles through preferred orientation thereby affecting the structure/morphology of the forming dendrites. So, this effect of surfactant can potentially be exploited to fine tune the structure/morphology of the dendrites.

In order to demonstrate the feasibility of such surfactant induced surface morphology engineering, we have performed the GRR of 50 mM $CuSO_4$ with Al foil and 100 mM HCl in presence of polyvinylpyrollidone (PVP) at various concentrations (100, 10, 1, and 0.1 mM). Figure 5(a-d) below shows the SEM images of the structures of the Cu deposit obtained at various PVP concentrations. For 100 mM PVP, the Cu deposits are characterized by random aggregates of small spherical shaped Cu particles (Fig. 5 a). At such high surfactant concentration, the Cu^{2+} can favorably interact with PVP to form a stable Cu^{2+} - PVP complex which would lead to reduced rate of nucleation.[49] Moreover, the presence of excess surfactant would coat the freshly nucleated Cu nanoparticles and would hinder their fusion with preferred orientation and would only form particles that undergoes clustering. Since the entire surface of the copper nuclei gets covered by PVP, the subsequent copper atoms deposit on an exposed Al foil rather than on a existing copper nuclei. Therefore a uniform layer of copper covers the foil completely as has been observed experimentally here while using high concentration of surfactant. This is in stark contrast to the observation of thick red deposits covering only certain regions of the Al foil during GRR in the absence of PVP. When the amount of PVP is reduced to 10 mM, the obtained Cu deposits clearly shows 1-D wire like growth pointed along the surface normal of the Al foil as shown in Figure 5 b. Here, the Cu nanoparticles have a modest tendency to fuse through self-assembly with preferred orientation and the structures resemble corncob like morphology. However, the reduced nucleation and growth rates restrict the successful formation of complete dendritic 2D structures with primary and secondary branches. This corncob like structures might actually represent the central trunk being formed with high degree of roughness due to incomplete fusion of the Cu nanoparticles that are covered (partially) with PVP.

Further decrease of PVP concentration to 1 mM starts to manifest tailoring of the structures of the Cu deposit. At this low concentration of PVP, the rate of nucleation and growth and the tendency to fuse and self assemble is expected to be greater than that of the case at 10 mM PVP. As shown in Figure 5 c, the Cu deposit represent a 'paddy like' networked structure with very short primary "branches" composed of tiny nanoparticles aggregated through self-assembly. This in effect shows that the experimental conditions now favor dendritic structures (although not fully grown). Interestingly, at 0.1 mM PVP concentration, the clear sign of size/morphology change of the dendrites are observed where dendritic like structures with many short branches, stretching in random directions, "cemented" to the trunk can be observed (Fig. 5 d). Some of the copper forms a smaller dendritic structures too. These dendrites possess a comparatively shorter side branching and are much smaller compared to dendrites prepared without any PVP. Even at such low concentrations of PVP, the obtained smaller sizes of these dendritic like structures clearly shows the effect of the surfactant on the structure/morphology of the obtained Cu dendrites. This effect of surfactant concentration on fine tuning the morphology of the Cu dendrites is anticipated to yield surface textured Cu structures with very high surface area and can be useful in variety of applications such as catalysis, wettability, and SERS based sensing..

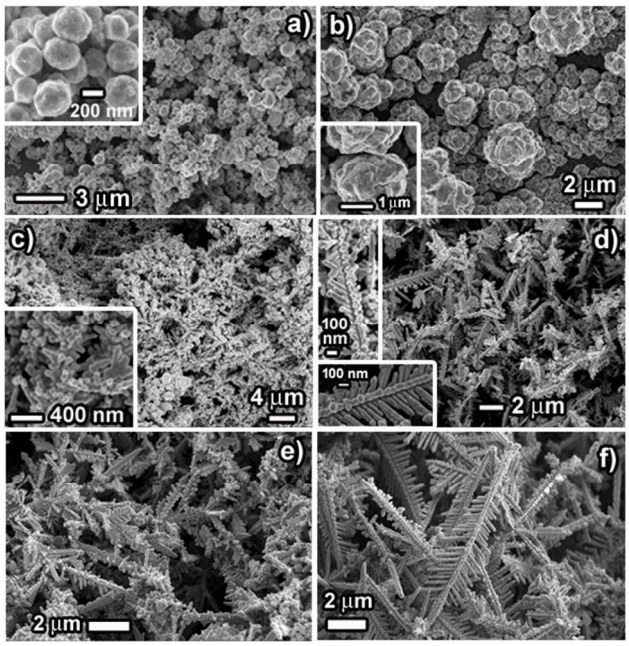

Figure 5. Effect of surfactant (a-d) and temperature (e-f) on the morphology/structure of the Cu dendrites. Copper dendrites prepared at room temperature using $CuSO_4$ (50 mM), HCl (100 mM) at varying concentrations (mM) of

PVP: a) 100, b) 10, c) 1, d) 0.1. The inset shows the higher magnification images of the structures formed. Cu dendrites prepared at 4° C using $CuSO_4$ (50 mM) with e) NaCl (100 mM) and f) HCl (100 mM).

Reaction Temperature: Reaction temperature is an important parameter that can affect the outcome of the product synthesis for the Cu dendrites using GRR strategy. It is anticipated that the rate of diffusion of nucleating Cu NPs, their migration and subsequent aggregation, cumulatively dictates mass transport during the growth of the dendritic structures. This rate of mass transport is expected to be slowed down at a lower reaction temperature. Hence, thermal field modifying the nucleation and growth rate can tailor the morphology of the obtained products. In order to probe the effect of the reaction temperature on the outcome of the product formation, we have carried out the GRR deposition of Cu structures on Al foil at a temperature lower than the room temperature. Figure 5 e, f shows the SEM images of the products obtained with $CuSO_4$ (50 mM) with NaCl/HCl (100 mM) at a reaction temperature of 4°C. Comparison of the SEM images of Figure 2 and 5 e, f reveals the effect of lowering the reaction temperature on the structure/morphology of the Cu dendrites. As can be clearly seen from Fig. 5 e, f, the Cu structures formed at 4 °C are strikingly different than the ones formed at room temperature (the other reaction parameters were held constant). For both the NaCl and HCl system, the Cu structures obtained at lower temperatures are far from being a fully grown dendrites and are smaller in sizes. Although the central backbone seems to have formed but the primary and secondary branches are far from being complete. The structures seem short, less dense, non-uniform and rough. The lowered reaction temperature reduces the diffusion based mass transport thereby restraining the movement of Cu nuclei which hinders the growth process of dendrites and finally leads to incomplete, short, rough and non-uniform dendritic structures.

Choice of Cu^{2+} precursor salt: The Cu dendrites that we have discussed up until now were fabricated using $CuSO_4$ as the precursor for Cu^{2+} ions. Do we expect any differences at all in the dendrite formation if we chose to use other Cu(II) salt such as Copper(II) Nitrate? Ideally, both $CuSO_4$ and $Cu(NO_3)_2$, when dissolved in water, is likely to form the same hydrated Cu^{2+} species. The UV-Vis spectra of $CuSO_4$ and $Cu(NO_3)_2$ solution are found to be identical (Figure S7, Electronic Supporting Information) and hence the reduction kinetics for $CuSO_4$ and $Cu(NO_3)_2$ is not expected to be strikingly different. This however, is strictly correct, if we assume that the counter anions (sulphates, nitrates) are merely spectator ions during the course of the dendrite formation reaction. No reports in the literature are found to explore the effect of the counter anions by choosing different Cu^{2+} precursor. In order to

understand the role played by the anions during the synthesis of dendrites, we have performed GRR using $Cu(NO_3)_2$ as the precursor salt while keeping the rest of the parameters constant (Al foil, NaCl/HCl 100 mM, $[Cu^{2+}]$: $[Cl^-]$ = 1:2, 1 hour reaction time). Surprisingly, we find that the yield of the reaction with nitrate counter anions are very low when compared to the corresponding sulphate case as depicted in Figure 6 a-d

This perplexing observation led us to further investigate the effect of the nitrate anions on the dendrite formation process. SEM image of the products formed with $Cu(NO_3)_2$ (50 mM), NaCl/HCl (100 mM) after 2 hours of reaction time at room temperature is shown in Figure S8 a, b; Electronic Supporting Information. It is clearly observable that no dendrite formation takes place when nitrate anions are the counter ions. Even after 12 hours of reaction time no dendrite formation was observed (Fig. S7 c, d; Electronic Supporting Information) albeit the yield of the Cu deposit increased. In order to further probe this effect of counter anions, we ran control experiments where we externally added Na_2SO_4 or $NaNO_3$ to $CuSO_4$ and $Cu(NO_3)_2$ reaction system. Specifically, when $NaNO_3$ is externally added to $CuSO_4$, HCl/NaCl system, we find very low yield of the reaction with no formation of dendritic morphology of the Cu deposit. The same holds true when Na_2SO_4 is added to $Cu(NO_3)_2$, HCl/NaCl system. Also, the reaction yield remains high when Na_2SO4 is added to $CuSO_4$, HCl/NaCl system. The corresponding photographs of the reaction vials are shown in Figure S9, Electronic Supporting Information. This led us to believe that the nitrate ions do play a key role and act as "poison" and heavily hampers the yield and formation of Cu dendrites.

In order to comprehend the underlying chemistry behind this "poisoning" effect of the nitrates, we have performed cyclic voltammetry (CV) experiments with $CuSO_4$ and $Cu(NO_3)_2$ as the reactants in presence of Na_2SO_4 as the background electrolyte under N_2 purging. Typical cyclic voltammogram of copper(II) sulphate and copper(II) nitrate systems at varying negative switching potentials ($-E_\lambda$) are presented in Figure 6 e-f. The cathodic process for both copper sulphate and copper nitrate system is evidenced by the peak in the negative current density region characterizing the reduction of Cu^{2+} to Cu^0. The anodic process for both copper sulphate and copper nitrate system is evidenced by the peak in the positive current density region which is due to the oxidation of Cu^0 to Cu^{2+} by the applied scanning potential. These voltammograms display crossover on the cathodic branches for both sulphate and nitrate systems which indicates that copper deposition proceeds via a nucleation and growth phenomena .[50-52] For the copper nitrate system in the cathodic and anodic region, the peaks are observed to slightly shift as the switching potential is varied. More interestingly, in the reduction region of the CV where $E < -0.3$ V, the nitrate systems

present a notable difference in the cathodic current after the metallic copper has been deposited. With the potential varying towards more negative values, the current keeps growing as observed for nitrate system. Such voltametric behaviors for nitrate systems indicate towards an additional supply of electroactive species on the reduction process. Such behavior has been previously observed for Cu[52], Co[51] reduction wherein a secondary chemical reaction of the freshly deposited metal with the nitrates have been observed. We believe that similar secondary chemical reaction involving the deposited Cu with the nitrates, that generates additional electroactive species, might be operative here in our case that leads to increasing cathodic current as the potential scans more negative values. This difference in the cathodic region for the sulphate vs. nitrate system indicates that the nitrate counter anions are far from being "spectator anions" and play an important chemical role during the deposition of metallic Cu.

In order to understand the effect of the nitrates on the yield of the Cu deposit, analysis of the cathodic efficiency of the Cu deposition was performed by a voltammetric study with different cathodic switching potentials ($-E_{-\lambda}$). The cathodic (Q_c) and anodic (Q_a) charges were calculated by integrating the cathodic and anodic branches of I vs. $-E_{-\lambda}$ curves respectively. This, in essence, reflects the amount of copper that undergoes oxidation from the electrode surface during the anodic scan by the applied potential. This charge deposition ratio can very well be utilized as a relative metric for ascertaining reaction yield of Cu deposits. Figure 6 g shows the plot of ratio of Q_a/Q_c against increasing negative switching potential for both copper sulphate and copper nitrate systems. The charge recovery for copper sulphate is around 0.9 (90%) indicating that almost all of the deposited copper is stripped away by the applied potential during the anodic scan. However for the copper nitrate system the charge recovery at a switching potential of -550 mV is low, around 0.52 (~52%). On further increasing the negative switching potential, the ratio goes down to 0.3 (30%). Therefore, low charge recoveries observed in the medium containing nitrate anions indicate an additional contribution that could be explained in terms of some process that can consume electrons or recently deposited Cu nuclei coupled to the cathodic reaction.

The only difference between the reactant composition is the presence of nitrate counter ions, it is likely that an interaction between newly deposited copper and nitrate ions in solution is occurring. The type of the interaction may include a direct redox reaction and/or nitrate reduction on the surface of the copper nuclei. The former reaction would consume the copper deposit, and the latter would provide electrons to the external circuit. Jointly or separately, these reactions explain the low copper recovery efficiency for a reactants containing nitrate counter ions. In fact, there are reports of electrodeposition of metals such as Copper[52], Cobalt[51], Thallium[53] during which the

nitrates have been found to interact with the freshly deposited metallic nuclei and undergo reduction thereby oxidizing the deposited metal and decreasing the yield of the metal deposit. The striking similarity between these prior observations during electrodeposition process and our electroless deposition process involving GRR on Al foil leads us to believe that the nitrate anions can act as an oxidant in a direct redox reaction with the freshly deposited Cu nuclei thereby decreasing the reaction yield of Cu deposits during our GRR deposition process. This nitrate augmented oxidative dissolution of the Cu nuclei will cause restrained nucleation and growth of the Cu deposit will be continuously interrupted. This reduced nucleation and growth rate hinders the kinetically controlled formation process of dendritic structures thereby affecting the morphology of the obtained Cu deposits as has been observed here in our case.

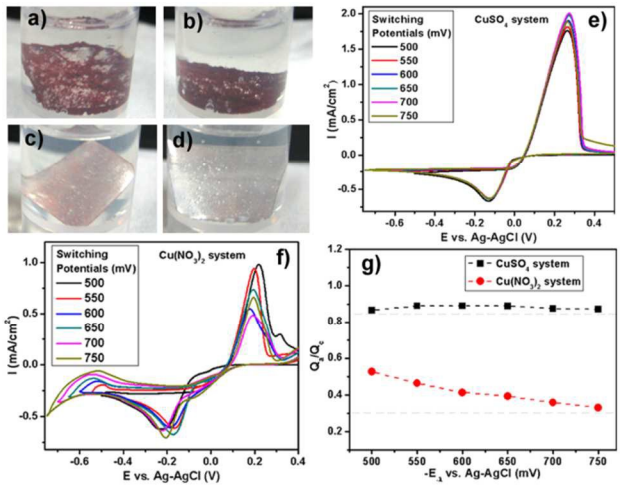

Figure 6: Photographs of Al foil immersed for 1 hour in vials containing a) $CuSO_4$ and HCl, b) $CuSO_4$ and NaCl, c) $Cu(NO_3)_2$ and HCl, d) $Cu(NO_3)_2$ and NaCl. Voltammograms obtained for different switching potentials at a scan rate of 20 mV/s for copper electrodeposition on GCE from e) $CuSO_4$, f) $Cu(NO_3)_2$, and g) Cathodic efficiency of Cu deposition (Q_a/Q_c) at various switching potentials ($-E_{-\lambda}$).

Applications: The fabricated dendrites, with high surface area and high nanostructuring, can be implemented for applications in catalysis and superhydrophobicity. Here we demonstrate the effective utilization of the Cu dendrites fabricated on Al foil using $CuSO_4$ (50 mM), HCl (100 mM) for these applications as these dendrites have higher surface texturing and are symmetrical with high self-similarity and uniformity. The dendrites fabricated using $CuSO_4$ (50 mM), NaCl (100 mM) have been used for these applications for comparison purposes.

Catalysis:

The catalytic activity of the as prepared Cu dendrites with high surface area was assessed by the model reduction reaction of 4-nitrophenol (NP) to 4-aminophenol (AP) in the presence of excess sodium borohydride ($NaBH_4$) at room temperature. A small aliquot of the reaction mixture was drawn out at regular intervals of time and was characterized spectrophotometrically. The amount of the reactant in the aliquot volume is insignificant as the utilized reactant solution volume is high with low concentration of NP. In the absence of the Cu dendritic catalysts, the reduction reaction is very slow and the mixture of NP and $NaBH_4$ shows a strong peak at 400 nm corresponding to the yellow-green color of the anionic 4-nitrophenolate species. This color of the 4-nitrophenolate anion strongly depends on the pH of the solution.[54] Hence, special care was taken during washing of the Cu dendrite catalysts to remove any remnant HCl (see experimental section). After the addition of the catalyst, the color of the solution gradually changes to colorless (Figure S10, Electronic Supporting Information). The strong 400 nm peak intensity decreases with the concomitant increase of the weak AP peak at 300 nm indicating the successful reduction of NP to AP catalyzed by the dendritic catalyst.

Figure 7 a, b, c shows the plot of the instantaneous absorbance as a function of reaction time for the various Cu structures utilized as catalyst here. As can be visually inferred that the apparent rate of the reduction reaction is fastest for Cu dendrites fabricated using HCl, followed by the Cu dendrites fabricated using NaCl, and then followed by the commercial Cu powder (Fig. 7 a, b, c). Since, $NaBH_4$ was present in excess during the reduction reaction, pseudo-first order kinetic analysis was performed to calculate the apparent rate constants for the three systems as shown in Fig 7 d. The observed linear relationship allows us to calculate the apparent rate constant (K_{app}) from the slope of the plots shown in Fig. 7 d. However, to compare the activities of the different solid catalysts, each k_{app} from the slope should be normalized to another comparable kinetic parameter, k_{nor} (mmol s^{-1} g^{-1}), according to the following equation[29]: $k_{nor} = (10^{-3} * C_0 * V/m) * k_{app}$; where C_0, V, and m are the initial concentration of 4-NP (mM), the volume of the reactant (4-NP) solution (mL), and the mass of catalyst (g), respectively. The normalized rate constants k_{nor} (mmol s^{-1} g^{-1}) for the Cu dendrites fabricated with HCl, NaCl, and commercial copper powder are found to be 18.2 x 10^{-3}, 6.1 x10^{-3}, and 1.9 x10^{-4} respectively.

The observed normalized rate constant for Cu dendrites obtained using NaCl are similar to earlier report[29]. However, it is interesting to find that the Cu dendrites fabricated using HCl have the highest normalized rate constant ever

reported. This indicates that increased nano-structuring may play a vital role in catalytic reduction reaction. The catalytic reduction process of 4-NP with $NaBH_4$ involves two steps: (1) diffusion and adsorption of 4-NP to metal surfaces and (2) electron transfer mediated by metal surfaces from $NaBH_4$ to 4-NP.[55, 56] Moreover, the first step is the rate determining step that has direct proportionality relation with available surface area. As discussed earlier in this report, the dendrites fabricated using HCl enjoys more nano-structuring/surface area than the ones prepared using NaCl (Fig. 2). Hence, the higher rate constant obtained for dendrites fabricated using HCl (Vs. NaCl) is attributed to their higher surface texturing/surface area. We thus believe that the nano-structured Cu dendrites obtained by our facile method are the promising candidates for the efficient catalytic reduction of nitrophenol compounds.

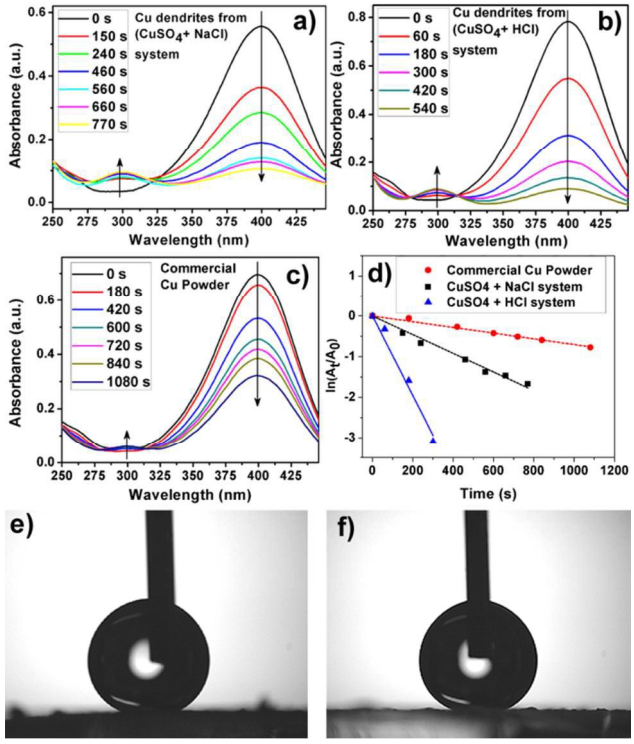

Figure 7. Reduction of 4-nitrophenol (NP) catalyzed by Cu dendritic structures prepared from 50 mM $CuSO_4$ and a) 100 mM NaCl , b) 100 mM HCl, c) commercial Cu Powder. D) Plot of ln (A_t/A_0) against time for the reduction of NP as obtained by monitoring absorbance at 400 nm. Static water contact angle (SWCA) measurement of films of n-dodecanethiol modified Cu dendrites prepared in presence of 50 mM $CuSO_4$ with e) 100 mM NaCl, f) 100 mM HCl exhibiting superhydrophobicity.

Superhydrophobicity:

Wettability of a surface is a basic property, when tailored, can be very useful for variety of applications such as self cleaning, anti-icing, anti-fogging, and antifouling.[57-59] Surface wettability for smooth surfaces is usually quantified in terms of static contact angle (CA) as defined by Young-Dupre equation (See Figure S11 a, Electronic Supporting Information). Contact angle hysteresis (CAH), that gives an indication of the stickiness of the surface, is the difference between the dynamic CAs measured during the growth (advancing; CA_a) and shrinkage (receding; CA_r) of a water droplet . Nature has plenty of examples of surfaces that are highly hydrophobic characterized with static water CA (SWCA) above 150°. Such surfaces are referred to as superhydrophobic surfaces and the classic example is a self-cleaning lotus leaf characterized by high SWCA (160°) and very low CAH (2°).[59] Inspired by nature's art of preparing superhydrophobic surfaces, researchers now know that the following surface parameters and their interplay have key roles in designing superhydrophobic surfaces: intrinsic hydrophobicity, surface morphology, and surface roughness.[58, 59] To obtain superhydrophobic surfaces with CA above 150°, it is imperative to have surface roughness. After physical micro/nano structuring of surfaces, a chemical post treatment with hydrophobic materials is performed routinely to lower the surface energy of the metallic structures.[58, 59] It is generally accepted that a low surface energy coating material needs to be present as the topmost layer on the surface of the material. Typically, utilized low energy coating material are flourinated or thiolated hydrocarbons. Such coatings turn the surface hydrophobic and help repel water from the surface. This hydrophobicity coupled with the presence of the surface roughness increases the air fraction present at the interface of liquid drop on the solid surface thereby acting as a cushion for suspending the liquid droplet resulting in increased CA.[58, 59]

The utility of the highly nanostructured Cu dendrites as a potential material for fabricating superhydrophobic surfaces was tested. Thoroughly washed Cu dendrites deposited on a PDDA-PSS functionalized glass slide are exposed to a solution of n-dodecanethiol, which acts as a low energy coating material, that renders the surface hydrophobic. Such films exhibit superhydrophobicity as observed by measurement of static contact angles with water droplet as probe liquid as shown in Figure 7 e-f. The Cu dendrites prepared using NaCl were found to have a static CA (CAH) of 151° (7°), while the Cu dendrites prepared in presence of HCl are found to have static CA (CAH) of 159° (2°). Clearly, both the surfaces are superhydrophobic in nature. Moreover, it is found that the water droplet cannot rest on and rolls off the n-dodecanethiol modified copper dendrite surface immediately, showing

great potential in self-cleaning applications. A corresponding real time video showing the water droplet rolling off of the surface is provided in the Electronic Supporting Information.

The observed differences in the CA for the Cu dendrites prepared using NaCl Vs. HCl primarily arise due to the inherent differences in the surface morphology and roughness of the dendrites as evidenced by their SEM analysis. The higher degree of roughness of the Cu dendrites prepared with HCl as compared to NaCl is thought to be the reason behind the differences in the measured static CA. The suspension of the water droplet on these nanostrcutured material is described by a composite state where the liquid-solid interface is now a composite of liquid-solid and liquid-vapor interface with increased air fraction due to increased nano-structured asperities. In such a scenario, the Cassie-Baxter model (CB model) can be qualitatively implemented. As per the CB model, the apparent contact angle can be expressed solely in terms of solid fraction for a given solid surface with CA θ (note that *apparent CA is directly proportional to solid fraction,* see Electronic Supporting Information Figure S11 b). The increased nano-structuring with increased air fraction with concomitant decrease of solid fraction then directly translates to increased apparent CA as expected from CB model. Clearly, the Cu dendrites prepared with HCl have higher nano-structuring than that of the NaCl ones and hence the former has higher SWCA. We believe that the surface textured Cu dendrites prepared by this simple method are efficient material for superhydrophobicity with self-cleaning abilities that may attract many pragmatic applications.

Conlusions:

Here, we present a simple, rapid, scalable, environment-friendly, and uninterrupted galvanic replacement reaction (GRR) based solution chemistry methodology to fabricate copper dendritic structures with tunable surface structure/morphology targeted towards desired applications. This facile methodology provides various reaction parameters that can be effectively utilized to control the deposition rate and surface morphology of the dendrites. The presence of the acid in the reaction system is demonstrated to have a profound effect on nano-structuring the dendrites. Moreover, we also find that the choice of Cu^{2+} precursor salt has a dramatic effect on the structure of the obtained copper deposits. Careful control of the other reaction parameters such as concentration of metal ions, concentration of surfactant, and reaction temperature also provides useful means of modulating the surface structure/morphology of the dendrites. Growth process of these dendrites have been probed by extensive temporal

SEM investigations. The acid induced nano-structured Cu dendrites show the highest ever reported normalized rate constant for the catalytic reduction of 4- nitrophenol (18.2 x 10^{-3} mmol s^{-1} g^{-1}). Wettability studies utilizing these nano-structured dendrites demonstrate excellent self-cleaning abilities due to superhydrophobicity with high static water contact angle and low contact angle hysteresis.

This report highlights how the underlying chemical reactions involved in the synthesis of these materials affect their material properties, and hence their application efficiency. The merits of our solution chemistry methodology and the properties of the synthesized Cu dendrites can be beneficially exploited for the production of low cost Cu nano/micro structures that can find practical applications as efficient catalysts and self-cleaning materials. Our ongoing efforts involve the utilization of dendritic structures with higher nanostructuring, as obtainable by modulating the other reaction parameters demonstrated here, for applications in catalysis, wettability, and Surface-enhanced Raman scattering (SERS) and Metal-enhanced Fluorescence (MEF) based chemical sensing.

Acknowledgements: Authors would like to acknowledge Dr. H. S. Panda, DIAT Pune for HRTEM images, Mr. A. B. Gaikwad for preliminary SEM imaging, Mr. S. S. Deo for acquiring XPS spectra. Authors would like to thank Prof. S. B. Ogale, Dr. P. A. Joy, and Dr. A. Nag for insightful discussions. This work was supported by DST grant number (SB/S2/RJN-61/2013) and CSIR-NCL start-up grant number (MLP 030326).

References:

1. Y. Xia and N. J. Halas, *MRS Bull*, 2005, **30**, 338-348.
2. F. Kim, S. Connor, H. Song, T. Kuykendall and P. Yang, *Angew. Chem. Int. Ed.*, 2004, **43**, 3673-3677.
3. J. Rongchao, C. Y. Charles, H. Encai, G. S. Metraux, G. C. Schatz and C. A. Mirkin, *Nature*, 2003, **425**, 487-490.
4. P. Lignier, R. Bellabarba and R. P. Tooze, *Chem. Soc. Rev.*, 2012, **41**, 1708-1720.
5. S. Habas, H. Lee, V. Radmilovic, G. Somorjai and P. Yang, *Nat. Mater.*, 2007, **6**, 692-697.
6. Y. Xia, Y. Xiong, B. Lim and S. E. Skrabalak, *Angew. Chem. Int. Ed.*, 2008, **48**, 60-103.
7. S. Lal, N. K. Grady, J. Kundu, C. S. Levin, B. Lassiter and N. J. Halas, *Chem. Soc. Rev.*, 2008, **37**, 898-911.
8. B. Wiley, Y. Sun, J. Chen, H. Cang, Z. Y. Li, X. Li and Y. Xia, *MRS Bull*, 2005, **30**, 356-361.
9. B. Wiley, Y. Sun and Y. Xia, *Acc. Chem. Res.*, 2007, **40**, 1067-1076.
10. B. K. Min and C. M. Friend, *Chem. Rev.*, 2007, **107**, 2709-2724.

11. A. Gutés, C. Carraro and R. Maboudian, *J. Am. Chem. Soc.*, 2010, **132**, 1476-1477.
12. M. H. Rashid and T. K. Mandal, *J. Phys. Chem. C*, 2007, **111**, 16750-16760.
13. W. Ren, S. J. Guo, S. J. Dong and E. K. Wang, *Nanoscale*, 2011, **3**, 2241-2246.
14. M. Matsushita, M. Sano, Y. Hayakawa, H. Honjo and Y. Sawada, *Phys. Rev. Lett.*, 1984, **53**, 286-290.
15. D. Barkey, F. Oberholtzer and Q. Wu, *Phys. Rev. Lett.*, 1995, **75**, 2980-2984.
16. W. J. T. A. and L. M. Sander, *Phys. Rev. Lett.*, 1981, **47**, 1400-1403.
17. S. R. Forrest and W. J. T. A., *J. Phys. A*, 1979, **12**, L109.
18. J. X. Fang, H. J. You, P. Kong, Y. Yi, X. P. Song and B. J. Ding, *Cryst. Growth. Des.*, 2007, **7**, 864-867.
19. Y. C. Han, S. H. Liu, M. Han, J. C. Bao and Z. H. Dai, *Cryst. Growth. Des.*, 2009, **9**, 3941-3947.
20. P. Meakin, *Phys. Rev. Lett.*, 1983, **51**, 1119.
21. M. Kolb, R. Botet and R. Jul-lien, *Phys. Rev. Lett.*, 1983, **51**, 1123.
22. G. X. Zhang, S. H. Sun, M. N. Banis, R. Y. Li, M. Cai and X. Sun, *Cryst. Growth. Des.*, 2011, **11**, 2493-2499.
23. H. P. Ding, G. Q. Xin, K. C. Chen, M. L. Zhang, Q. Y. Liu, J. C. Hao and H. G. Liu, *Colloid Surface A*, 2010, **353**, 166-171.
24. R. Qiu, H. G. Cha, H. B. Noh, Y. B. Shim, X. L. Zhang, R. Qiao, D. Zhang, Y. I. Kim, U. Pal and Y. S. Kang, *J. Phys. Chem. C*, 2009, **113**, 15891-15896.
25. W. Shao and G. Zangari, *J. Phys. Chem. C*, 2009, **113**, 10097-10102.
26. B. K. Barman and K. K. Nanda, *Dalton Trans.*, 2015, **44**, 4215-4222.
27. S. Sun, C. Kong, L. Wang, S. Yang, X. Song, B. Ding and Z. Yang, *CrystEngComm*, 2011, **13**, 1916-1921.
28. C. Yan and D. Xue, *Cryst. Growth. Des.*, 2008, **8**, 1849-1854.
29. J. Liu, Q. Wu, F. Huang, H. Zhang, S. Xu, W. Huang and Z. Li, *RSC Advances*, 2013, **3**, 14312-14321.
30. W. Ye, Y. Chen, F. Zhou, C. Wang and Y. Li, *J. Mater. Chem.*, 2012, **22**, 18327-18334.
31. J. Y. Zheng, A. P. Jadhav, G. Song, C. W. Kim and Y. S. Kang, *Thin Solid Films*, 2012, **524**, 50-56.
32. K. H. Kim, J. Y. Zheng, W. Shin and Y. S. Kang, *RSC Adv.*, 2012, **2**, 4759-4767.
33. J. Y. K. Zheng, M. J., G. Song, S. I. Son, S. P. Suh, C. W. Kim and Y. S. Kang, *CrystEngComm*, 2012, **14**, 6957-6961.
34. R. Qiu, J. Y. Zheng, H. G. Cha, M. H. Jung, K. J. Lee and Y. S. Kang, *Nanoscale*, 2012, **4**, 1565-1567.
35. A. Sinha and B. P. Sharma, *Mater. Res. Bull.*, 2002, **37**, 407-416.
36. M. D. Susman, Y. Feldman, A. Vaskevich and I. Rubinstein, *Chem. Mater.*, 2012, **24**, 2501-2508.
37. Y. Wang, A. V. Biradar, G. Wang, K. K. Sharma, C. T. Duncan, S. Rangan and T. Asefa, *Chem. Eur. J.*, 2010, **16**, 10735-10743.
38. A. Sarkar, T. Mukherjee and S. Kapoor, *J. Phys. Chem. C*, 2008, **112**, 3334-3340.
39. M. Jin, G. He, H. Zhang, J. Zeng, Z. Xie and Y. Xia, *Angew. Chem. Int. Ed.*, 2011, **50**, 10560-10564.
40. X. J. Zhang, G. F. Wang, X. W. Liu, W. H. Q. and B. Fang, *Cryst. Growth. Des.*, 2008, **8**, 1430-1434.
41. J. Fu, W. Ye and C. Wang, *Mater. Chem. Phys.*, 2013, **141**, 107-113.
42. Q. Wu and D. Barkey, *J Electrochem. Soc.*, 2000, **147**, 1038-1045.
43. Y. Zhang, S. Sun, X. Zhang, L. Tang, X. Song and Z. Yang, *Phys. Chem. Chem. Phys.*, 2014, **16**, 18918-18925.
44. R. M. Brady and R. C. Ball, *Nature*, 1984, **309**, 225-229.
45. J. Xu and D. Xue, *J. Phys. Chem. B*, 2006, **110**, 11232-11236.
46. J. Fang, B. Ding and X. Song, *Cryst. Growth Des.*, 2008, **8**, 3616-3622.
47. J. Fang, X. Ma, H. Cai, X. Song and B. Ding, *Nanotechnology*, 2006, **17**, 5841-5845.
48. J. Fang, B. Ding, X. Song and Y. Han, *Appl. Phys. Lett.*, 2008, **92**, 173120.
49. I. Haas, S. Shanmugam and A. Gedanken, *J. Phys. Chem. B*, 2006, **110**, 16947-16952.
50. S. Fletcher, *Electrochim. Acta*, 1983, **28**, 917-923.

51. E. Barrera, M. P. Pardavé, N. Batina and I. González, *J Electrochem. Soc.*, 2000, **147**, 1787-1796.
52. A. Ramos, M. Miranda-Hernández and I. González, *J Electrochem. Soc.*, 2001, **148**, C315-C321.
53. A. Serruya and B. R. Scharifker, *in Extended abstracts of the Tenth Congreso de la Sociedad Venezolana de Electroquímica,*, 1997, P. 57.
54. J. Zeng, Q. Zhang, J. Chen and Y. Xia, *Nano Lett.*, 2009, **10**, 30-35.
55. K. Esumi, K. Miyamoto and T. Yoshimura, *J. Colloid Interface Sci.*, 2002, **254**, 402-405.
56. K. Hayakawa, T. Yoshimura and K. Esumi, *Langmuir*, 2003, **19**, 5517-5521.
57. T. C. Rangel, A. F. Michels, F. Horowitz and D. E. Weibel, *Langmuir*, 2015, **31**, 3465-3472.
58. T. Darmanin, E. T. Givenchy, S. Amigoni and F. Guittard, *Adv. Mater.*, 2013, **25**, 1378-1394.
59. X.-M. Li, D. Reinhoudt and M. Crego-Calama, *Chem. Soc. Rev.*, 2007, **36**, 1350-1368.

Table of Contents Figure:

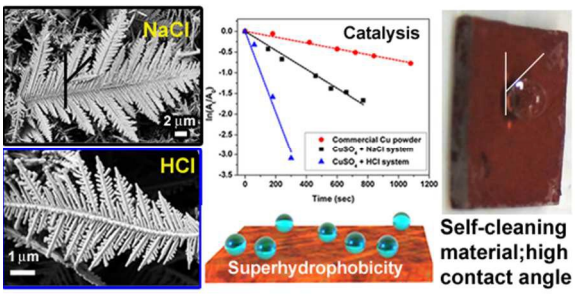

Graphic Abstract: Solution chemistry based nano-structuring of Cu dendrites is exploited to enhance their efficiency in applications of catalysis and superhydrophobicity.